HHS Public Access

Author manuscript

Nature. Author manuscript; available in PMC 2019 July 11.

Published in final edited form as:

Nature. 2018 July ; 559(7715): 580–584. doi:10.1038/s41586-018-0331-8.

Cryo-EM structures of fungal and metazoan mitochondrial calcium uniporters

Rozbeh Baradaran[1,3], **Chongyuan Wang**[1,3], **Andrew Francis Siliciano**[1,2], and **Stephen Barstow Long**[1,*]

[1]Structural Biology Program, Memorial Sloan Kettering Cancer Center, New York, NY, USA.

[2]Weill Cornell/Rockefeller/Sloan Kettering Tri-Institutional MD-PhD Program, New York, NY, USA.

[3]These authors contributed equally: Rozbeh Baradaran, Chongyuan Wang.

Abstract

The mitochondrial calcium uniporter (MCU) is a highly selective calcium channel and a major route of calcium entry into mitochondria. How the channel catalyses ion permeation and achieves ion selectivity are not well understood, partly because MCU is thought to have a distinct architecture in comparison to other cellular channels. Here we report cryo-electron microscopy reconstructions of MCU channels from zebrafish and Cyphellophora europaea at 8.5 Å and 3.2 Å resolutions, respectively. In contrast to a previous report of pentameric stoichiometry for MCU, both channels are tetramers. The atomic model of C. europaea MCU shows that a conserved WDXXEP signature sequence forms the selectivity filter, in which calcium ions are arranged in single file. Coiled-coil legs connect the pore to N-terminal domains in the mitochondrial matrix. In C. europaea MCU, the N-terminal domains assemble as a dimer of dimers; in zebrafish MCU, they form an asymmetric crescent. The structures define principles that underlie ion permeation and calcium selectivity in this unusual channel.

The Ca^{2+} channel of the inner mitochondrial membrane, known as the mitochondrial calcium uniporter (MCU), enables mitochondria take up substantial amounts of Ca^{2+} from the cytosol during intracellular Ca^{2+} signalling events[1–5]. Ca^{2+} influx stimulates mitochondrial ATP synthesis, controls the mitochondrial permeability transition that leads to

* longs@mskcc.org.

Author Contributions R.B. and C.W. performed cryo-EM studies of CeMCU and zebrafish MCU, respectively, and other experiments. A.F.S. developed MCU and EMRE double knockout cells. S.B.L. directed the research and assisted with cryo-EM. All authors contributed to data analysis and the preparation of the manuscript.

Online content Any Methods, including any statements of data availability and Nature Research reporting summaries, along with any additional references and Source Data files, are available in the online version of the paper at

Reviewer information *Nature* thanks P. Yuan and the other anonymous reviewer(s) for their contribution to the peer review of this work.

Competing interests: The authors declare no competing interests.

Additional information

Reprints and permissions information is available at www.nature.com/reprints.

Publisher's note: Springer Nature remains neutral with regard to jurisdictional claims in published maps and institutional affiliations.

Data availability. Atomic coordinates of CeMCU have been deposited in the PDB under accession 6DNF. The three-dimensional cryo-EM density maps have been deposited in Electron Microscopy Data Bank under accessions EMD-7971 (CeMCU) and EMD-7972 (zebrafish MCU).

cell death, and acts in a buffering role to shape cytosolic calcium signals[6]. A negative electric potential (approximately −160 mV) of the mitochondrial matrix relative to the cytosol, which is established by the proton gradient across the inner membrane, is the driving force for Ca^{2+} influx[7]. MCU is one of the most Ca^{2+}-selective channels known[8] and must be highly discriminatory to enable the uptake of Ca^{2+} while excluding other cytosolic cations, of which potassium is more than 100,000 times more abundant ($[Ca^{2+}]_{cytosol} \approx 0.1–1$ μM and $[K^{+}]_{cytosol} \approx 150$ mM). The selectivity of MCU is of paramount importance because substantial cation leakage could collapse the electromotive force used for ATP synthesis. It is thought that selectivity is achieved, in part, by high-affinity binding of Ca^{2+} (dissociation constant (K_d) ≤ 2 nM) within a 'selectivity filter' region of the pore[8]. The selectivity filter might involve a conserved signature sequence (WDXXEP) near the channel's two predicted transmembrane helices[3,4], but its 3D conformation is not known, partly because MCU shares no apparent sequence similarity to other ion channels. Ca^{2+} ions can move rapidly through the pore of MCU (maximally at about 5×10^6 Ca^{2+} s^{-1})[8], and this raises the apparent paradox of how both ion selectivity and high conductance are achieved.

MCU channels are present in most clades of eukaryotic life, including protists, plantae, amoebozoa, fungi, and metazoa[9]. The MCU protein subunit oligomerizes to form the Ca^{2+}-conducting pore[3–5], but channel activity is regulated differently among clades. Metazoans require the single-pass transmembrane protein EMRE for Ca^{2+} uptake, whereas the genomes of fungi, amoeba, and plants do not have a recognizable EMRE orthologue[10]. Many MCU channels are further regulated by MICU1 and MICU2 proteins, which are present in the intermembrane space[11,12], and by the protein MCUR1[13–15]. The structures of MCU from zebrafish and the fungus *C. europaea* presented here define the architecture of the channel and give insight into the mechanisms of ion permeation and Ca^{2+} selectivity.

Structure determination and oligomeric state

C. europaea MCU (CeMCU) and zebrafish MCU have 44% and 91% sequence similarity to human MCU, respectively, and were selected for structural determination on the basis of good biochemical stability in detergent-containing solutions (see Methods, Extended Data Fig. 1). Zebrafish MCU catalyses mitochondrial Ca^{2+} uptake when co-expressed with EMRE (Extended Data Fig. 2a–c). Uptake is blocked by ruthenium-red and is dependent upon the proton gradient. Thus, zebrafish MCU recapitulates known properties of the human channel[3,16].

An orthologue of EMRE has not been identified in the genome of *C. europaea*. MCU channels from *Dictyostelium discoideum* and *Arabidopsis thaliana*, two other species without an EMRE, can mediate mitochondrial Ca^{2+} uptake when heterologously expressed[16,17]. However, we did not observe uptake when CeMCU or several other fungal MCU channels were expressed in yeast or mammalian cells, and conjecture that at least a subset of fungal channels may be regulated differently from other MCU channels.

For cryo-electron microscopy (cryo-EM) sample preparation, full length CeMCU and zebrafish MCU were produced using eukaryotic expression systems and purified using gentle, non-denaturing, methods. In a previous NMR study of a truncated version of

Caenorhabditis elegans MCU lacking an N-terminal domain (NTD), which resulted in a different structure from the one presented here[18], a prokaryotic system was used for expression and purification involved a relatively harsh detergent (foscholine-14), which is rarely used in structural studies of membrane proteins[19].

The small molecular weight of MCU, just approximately 110 kDa for the ordered region of the channel assembly, poses challenges for structure determination by cryo-EM. We overcame these by collecting micrographs at high magnification and high total electron dose (see Methods). De novo initial 3D models of CeMCU and zebrafish MCU were generated independently and refined without imposing symmetry in order to avoid bias with regard to oligomeric state or overall structure (Extended Data Figs. 3, 4). The 3D reconstructions demonstrate that both channels assemble as tetramers of subunits (Figs. 1, 2). 3D classification of the particle images, which would reveal global differences such as differences in oligomeric state, consistently yielded reconstructions that were tetrameric (Extended Data Figs. 3, 4). A tetrameric oligomeric state is supported by crosslinking experiments of purified protein and of human MCU within mitochondrial membranes (Extended Data Fig. 2h–j). The 3D reconstructions of CeMCU and zebrafish MCU were determined at overall resolutions of 3.2 Å and 8.5 Å, respectively (Figs. 1, 2 and Extended Data Figs. 5, 6). Density for most amino acid side chains of CeMCU allowed us to construct an atomic model with good stereochemistry and good correlation with the cryo-EM density (Fig. 1, Extended Data Fig. 6 and Extended Data Table 1). Because of the higher resolution, the discussion of atomic details that follows derives from CeMCU. Although individual α-helices cannot be resolved in the map of zebrafish MCU, aside from differently organized NTDs, the overall structures of zebrafish MCU and CeMCU are similar (Figs. 1, 2).

Overall architecture

MCU has a novel architecture for an ion channel (Fig. 1, Extended Data Fig. 7). The molecular surface contains a hydrophobic transmembrane domain (TMD) that would reside within the inner mitochondrial membrane in a cellular setting and a large hydrophilic region in the matrix (Extended Data Fig. 7d). The TMD has four-fold symmetry (Figs. 1, 2) with eight transmembrane helices (the two transmembrane helices (TM1 and TM2) from each of the subunits (Fig. 1)). The transmembrane helices interact through mostly hydrophobic amino acids (Extended Data Fig. 7g). Short ‘turrets’ connecting these helices are the only protrusions into the intermembrane space. On the matrix side, four ‘legs’ extend from the TMD. The legs are composed of an N-terminal extension of the TM1 helix ($TM1_{ext}$) and a C-terminal helix (α6) that forms a coiled-coil with it in the matrix (Fig. 1c, Extended Data Fig. 7a). Sequence analysis indicates that all MCU channels contain analogous coiled-coil regions[9]. The legs are separated from one another, creating ample space for ions to diffuse between them in the matrix. An NTD, which each MCU orthologue is predicted to contain[9], is located at the end of each of the legs, approximately 70 Å from the membrane. In CeMCU, the four NTDs are arranged as a dimer of dimers, and this yields an overall two-fold (*C*2) symmetry for the channel (Fig. 1). In zebrafish MCU, the four NTDs are arranged as an asymmetric crescent (Fig. 2). Thus, in both channels, there is a symmetry transition between the four-fold symmetric TMD and the matrix region. The cryo-EM structures differ

substantially from the structural model of MCU that was deduced from NMR experiments[18] both on the subunit level and in terms of its assembly (Extended Data Fig. 8).

Ion pore

MCU contains a single ion pore in the TMD that is located along the symmetry axis and would be perpendicular to the membrane in a cellular setting (Figs. 1, 3). The secondary structure of the channel is entirely α-helical within the TMD; amino acid side chains emanating from α-helices form the walls of the pore. The pore can be divided into two portions: a narrower portion that occupies the outer leaflet of the membrane and contains the selectivity filter and a wider 'vestibule' portion located in the inner leaflet (Fig. 3). In the outer leaflet, TM2 lines the pore and TM1 is located at the periphery, whereas both TM1 and TM2 line the vestibule. The WDXXEP signature sequence (WDVMEP in CeMCU) adopts an α-helical secondary structure within TM2, forming three turns of this helix with the W residue (Trp224) at its N-terminal end. The side chains of the D and E residues (Asp225 and Glu228) protrude into the pore. The W and P residues (Trp224 and Pro229) are tightly packed and generally oriented towards the pore, although they are not expected to interact with Ca^{2+}. The X residues (Val226 and Met227), face away from the pore and would be exposed to the membrane in a cellular setting (Fig. 4b). Pro229 induces a slight bend in the TM2 helix owing to local disruption of the α-helical hydrogen bonding (Fig. 4b).

To assess the relevance of the conformation of the WDXXEP sequence observed in CeMCU to human MCU, we introduced alanine and other mutations at each position of the signature sequence of human MCU (WDIMEP) and evaluated mitochondrial Ca^{2+} uptake of the mutants by co-transfecting with wild-type human EMRE in mammalian cells in which the endogenous MCU and EMRE genes had been disrupted (MCU/EMRE knockout cells). Consistent with a pattern predicted by the structure, and with previous mutagenesis of the acidic amino acids[3], Ca^{2+} uptake was not observed when pore-oriented amino acids (W, D, E, or P) were mutated, but was observed for mutants of either X residue, which face the membrane in the structure of CeMCU (Fig. 4d and Extended Data Fig. 2d–g). The first X residue, Ile262 of human MCU, was particularly insensitive to mutation. The corresponding side chain of CeMCU (Val226) has no protein contacts in the structure. Both the I262V mutant, in which the signature sequence is converted to that of CeMCU, and the I262A mutant had full activity. M263A showed diminished but significant activity relative to the wild type, and this is consistent with the observation that while Met227 of CeMCU faces the membrane it also interacts with TM1 (Fig. 4b). These data support the conclusion that the signature sequence adopts similar conformations in metazoan and fungal MCU channels.

Selectivity filter

The selectivity filter is formed by symmetrical arrangement of WDXXEP signature sequences around the pore (Fig. 4). This region is both the narrowest portion of the pore and the only one that is lined by acidic amino acids. Its α-helical secondary structure is distinct from channels belonging to the superfamilies of CaV, NaV, Kv, TRP, RyR, and IP3R cation channels, which possess loop-like secondary structures within their selectivity filters[20–27]. The D (Asp225) residues of the tetrameric channel form an acidic mouth on the side of the

pore facing the intermembrane space, giving the pore a radius of approximately 2.2 Å in this region (Fig. 3). The E (Glu228) residues form a second acidic ring, with a pore radius of less than 1 Å (Fig. 3). These glutamate residues extend fully away from the helical axis of TM2 and point towards the centre of the pore (Fig. 4c). The substitution of an aspartate residue would markedly change the pore dimensions. Accordingly, the corresponding E264D mutation of human MCU is defective in mitochondrial Ca^{2+} uptake[18]. Each W side chain (Trp224) is oriented down such that it interdigitates with the Glu228 side chains and appears to stabilize the conformation of the selectivity filter from behind (Fig. 4b, c). Each W side chain also packs against the P (Pro229) residue from a neighbouring subunit and makes both van der Waals interactions and hydrogen bonds with neighbouring E (Glu228) side chains (Fig. 4c). The W residue is particularly sensitive to mutation; Ca^{2+} uptake was not observed for any of the mutants tested (alanine, phenylalanine or tyrosine; Fig. 4d).

Ca^{2+} binding

Roughly spherical density is located at three sites in the upper portion of the pore (Fig. 4a). The sites are evenly spaced approximately 6 Å apart and located on the symmetry axis. Densities in site 1 and site 2 are within the selectivity filter and can be ascribed to Ca^{2+} on the basis of their chemical environment. Density in site 3, which is located in the upper portion of the vestibule, is harder to assign as it is approximately 6 Å away from the surrounding Thr231 and Tyr232 residues (measured to atom centres) and may represent Ca^{2+} or another small molecule. Site 1 is positioned in the centre of the ring of Asp225 residues. The distance between site 1 and each Asp225 carboxylate is approximately 4 Å (between atom centres), which suggests water-mediated interactions with these side chains. Site 2 is located within the ring of Glu228 residues and only about 2.3 Å from their carboxylates, indicating direct coordination.

The surface of the channel facing the intermembrane space is strongly electronegative (Extended Data Fig. 7e). In addition to the ring of Asp225 residues surrounding site 1, Asp221 (Glu257 in human MCU) is present on each turret (Fig. 3). The preponderance of electronegativity would tend to concentrate cations at the entrance to the pore. We envision the following scenario. A Ca^{2+} ion reaching the pore would remain hydrated in site 1. As it moves inward towards site 2 it would shed water to directly interact with the ring of Glu228 residues, perhaps retaining axial water molecules above and below it. On the basis of this direct coordination, and as site 2 has the strongest density in the entire cryo-EM map (Fig. 4a), we suspect that site 2 represents the high-affinity binding site for Ca^{2+} in MCU. After emerging from the selectivity filter, a Ca^{2+} ion could become more hydrated in the vestibule (for example, in site 3). We hypothesize that ion selectivity for Ca^{2+} involves a knock-off mechanism between sites 1 and 2. In this mechanism, a Ca^{2+} ion moving inward from site 1 would displace the Ca^{2+} ion in site 2 into the vestibule, and site 1 would be refilled from the intermembrane space. Such a mechanism, involving multiple ions in single file, can allow rapid ion throughput in the context of high selectivity[28].

Site 2 may underlie another characteristic of MCU. Unlike many Ca^{2+} channels that efficiently conduct both Na^+ and potassium K^+ when Ca^{2+} and other divalent cations are removed, MCU efficiently conducts Na^+ but not K^+ under these conditions[8]. The

dimensions of the selectivity filter at site 2 may explain this electrophysiological hallmark. We hypothesize that Na^+ could pass through site 2 when it is not occupied by Ca^{2+} because Na^+ and Ca^{2+} have nearly the same ionic radius (1.02 Å and 1.00 Å, respectively). On the other hand, K^+ has an ionic radius of 1.38 Å and would be too large to fit in site 2. Correspondingly, the selectivity filter in K^+ channels is slightly wider than in MCU. In the K^+ channel KcsA[29], for example, the oxygen atoms of the selectivity filter that coordinate K^+ are separated by 4.7 Å across the pore in comparison to approximately 3.9 Å separation in MCU (measured between atom centres). This discrimination on the basis of size is an indication that the selectivity filter of MCU is relatively rigid at site 2. We postulate that site 2 preferentially binds Ca^{2+} over Na^+ because its +2 charge is better matched to direct coordination by the glutamate residues, and that site 2 would be constitutively occupied by Ca^{2+} under cellular conditions. When sites 1 and 2 are occupied, the local concentration of Ca^{2+} in the selectivity filter would be approximately 8 M (2 ions in a volume of approximately 4×10^{-25} l), which is more than 10 million times the concentration of Ca^{2+} in the cytosol. Selectivity for Ca^{2+} in MCU appears to be a combination of attractive, repulsive and excluded-volume forces.

The N-terminal domains

Each individual NTD of CeMCU adopts the same structure (Cα root mean square deviation (r.m.s.d.) = 0.5 Å), and superposes with X-ray structures of isolated NTDs of human MCU (Cα r.m.s.d. = 2 Å)[30,31], despite 16% sequence identity (Extended Data Fig. 9a). Inspection of the crystal lattice from the X-ray structures reveals an arrangement of NTDs that is similar to the crescent we observe in the structure of the full-length zebrafish channel (Extended Data Fig. 9b, c). This correspondence suggests that the NTDs of human MCU adopt a similar organization in the assembled channel. We find that, like human MCU[18,30], zebrafish MCU can catalyse Ca^{2+} uptake without an NTD (Extended Data Fig. 2a–c). Nevertheless, it is possible that the NTDs have regulatory properties, which may include modulation by matrix cations[31] and binding of MCUR1[30].

Membrane interactions

Densities ascribed to four lipid molecules (on the basis of shape and position) are located on the membrane-exposed surfaces adjacent to the TM2 helices (Fig. 5a). Although the type of lipid cannot be discerned from the density, the lipids would belong to the outer leaflet and are oriented in a conventional manner with their head groups facing the intermembrane space.

Within the inner leaflet, TM1 and TM2 are separated by a few Ångstroms and this creates lateral membrane openings (‘fenestrations’) in the transmembrane molecular surface that would expose the vestibule to the membrane (Fig. 5a). Four horizontally oriented tubes of density consistent with acyl chains of lipid molecules are observed within the fenestrations just below site 3 (Fig. 5a, b). The densities are positioned similarly to acyl chains observed in fenestrations of certain other cation channels, including two-pore domain potassium channels and a voltage-dependent sodium channel[21,32–34]. A minor conformational change in the transmembrane helices, such as a hinge-like motion at or near Gly235 on TM2 (Fig.

3), could seal the fenestrations, raising hypotheses regarding possible ion permeation and gating mechanisms and the potential involvement of lipids in them.

Discussion

The presence of lipids in the vestibule might prevent ion permeation, and thus a wider lower portion of the channel, as observed in CeMCU, may represent a non-conductive ('closed') conformation of the channel. On the other hand, with its wide vestibule, the structure may represent a conductive conformation. If this is the case, perhaps lipids are involved in the inward rectification exhibited by MCU, wherein the channel preferentially catalyses the flow of Ca^{2+} towards the matrix[8]. In this mechanism, Ca^{2+} ions emerging from the selectivity filter into site 3 would be pulled inward by the voltage gradient across the membrane and could transiently displace lipids along their path through the vestibule. Ca^{2+} ions would not have sufficient potential energy to efficiently pass through the lipids without the negative voltage of the matrix. In the absence of inward ion flow, the vestibule could fill with lipids and MCU would present itself to the matrix as collection of transmembrane helices with intervening lipids rather than an aqueous pore. These lipids 'covering up' the selectivity filter would tend to prevent outward ion flow and this would be manifest to the experimentalist as inward rectification when applying a positive voltage inside the matrix. The legs of the channel appear suited to allow lipid movement. Entire lipid molecules of the inner leaflet, along with their head groups, could diffuse in and out of the vestibule between the legs. In line with this hypothesis, the surfaces of TM1 and TM2 lining the vestibule are hydrophobic and basic residues on the legs appear poised to interact with phospholipid head groups (Fig. 5c). Analogous residues are present in human MCU (Extended Data Fig 1). The structure establishes a foundation to probe lipid involvement.

The structures of zebrafish MCU and CeMCU reveal a new architecture for a Ca^{2+} channel. The pore of MCU differs from the large superfamily of cation channels, which have a pore architecture first observed for a K^+ channel[35]. Unlike those channels that have loop-like secondary structures in their selectivity filters, the selectivity filter of MCU is formed by α-helices that coordinate Ca^{2+} with rings of acidic amino acids. The structures suggest that MCU combines a multi-ion selectivity filter, a discriminatory Ca^{2+} binding site, an electronegative surface exposed to the intermembrane space, and a vestibule to lower energy barriers for Ca^{2+} influx into mitochondria and achieve high selectivity for Ca^{2+}. They also indicate potential sites of channel regulation, not only by EMRE, MICU1 and MICU2 in the membrane and intermembrane space but also by other functionalities within the matrix.

METHODS

Cloning, expression and purification of CeMCU

Cyphellophora europaea MCU (CeMCU; UniProt accession W2SDE2) was selected as a candidate for structural studies from among numerous MCU orthologues that were evaluated using fluorescence-detection size-exclusion chromatography (FSEC) with HEK-293 cells[36]. The cDNA of CeMCU (synthesized by BioBasic) was ligated into the EcoRI–SalI restriction sites of the *Pichia pastoris* expression vector pPICZ-C (Invitrogen Life Technologies), encoding the full-length protein followed by a C-terminal antibody-affinity tag (GEGEEF)

that is recognized by the anti-tubulin antibody YL1/2[37]. Transformation into *P. pastoris* (SMD1168 strain, Invitrogen), expression and cryo-lysis were performed as previously described[38].

Mild detergents (n-dodecyl-β-D-maltoside and digitonin) that are commonly used for structural studies of membrane proteins[19] were used for preparation of CeMCU and zebrafish MCU. All purification steps were carried out at 4 °C. For CeMCU, lysed *P. pastoris* cells (~150 g) were re-suspended in 1.5 L of RB buffer containing 20 mM 4-(2-hydroxyethyl)-1-piperazineethanesulfonic acid (HEPES), pH 7.5, 150 mM NaCl, 1 mM $CaCl_2$, 0.15 mg/mL DNase I (Sigma-Aldrich), 1.5 μg/mL Leupeptin (Sigma-Aldrich), 1.5 μg/mL Pepstatin A (Sigma-Aldrich), 1 mM Benzamidine (Sigma-Aldrich), 1 mM 4-(2-aminoethyl) benzenesulfonyl fluoride hydrochloride (AEBSF, Gold Biotechnology), 1 mM phenylmethanesulfonyl fluoride (PMSF, Acros Organics) and 1:500 dilution of Aprotonin (Sigma-Aldrich). Cell debris was removed by centrifugation (3 × 7000*g* for 20 min), and cellular membranes were collected by centrifugation at 43,000*g* for 20 min. The pelleted membranes were resuspended in 100 mL of RB buffer supplemented with 20% (v/v) glycerol, flash-frozen in liquid nitrogen, stored at −80 °C. Membranes (~33 mL, corresponding to ~40 g of lysed cells) were thawed, diluted with equal volume of RB buffer, and solubilized with 2 g of n-dodecyl-β-maltoside (DDM, Anatrace) by rotating for 1 h at 4 °C. The sample was then centrifuged at 43,000*g* for 45 min and the supernatant was filtered through a 0.22-μm polystyrene membrane (Millipore). YL1/2 antibody (IgG, expressed from hybridoma cells and purified by ion-exchange chromatography using standard methods) was coupled to CNBr-activated Sepharose beads (GE Healthcare) according to manufacturer's protocol. Approximately 0.4 mL of YL1/2 antibody beads were added to the sample for each 1 g of *P. pastoris* cells and the mixture was rotated at 4 °C for 1 h. Antibody beads were collected on a column support, washed with ~5 column volumes of a buffer containing 20 mM HEPES, pH 7.5, 150 mM NaCl, 1 mM $CaCl_2$, 2 mM DDM and 0.1 mg/mL 1',3′-bis[1,2-dioleoyl-*sn*-glycero-3-phospho]-*sn*-glycerol (18:1 cardiolipin, Avanti Polar Lipids), and the protein was eluted with a buffer containing 100 mM HEPES, pH 7.5, 150 mM NaCl, 1 mM $CaCl_2$, 2 mM DDM, 0.1 mg/mL cardiolipin and 1 mM Glu-Glu-Phe peptide (Peptide 2.0). The elution fraction was concentrated to ~5 mg/mL using a 100 kDa concentrator (Amicon Ultra; EMD Millipore) and run on a Superose-6 10/300 Increase size-exclusion chromatography (SEC) GL column, equilibrated with a buffer containing 20 mM HEPES pH 7.5, 150 mM NaCl, 1 mM $CaCl_2$, 0.5 mM digitonin (Cayman Chemical Company) and 0.05 mg/mL cardiolipin. (Digitonin was used at the end of the purification procedure because it produced more uniform ice on the cryo-EM grids than DDM.) The elution fractions containing the CeMCU protein were pooled and concentrated to ~5 mg/mL using a 100 kDa concentrator (Vivaspin-2). Purified protein was used immediately for cryo-Electron Microscopy (cryo-EM) grid preparation.

Cloning, expression and purification of zebrafish MCU

Danio rerio (zebrafish) MCU was selected as a candidate for structural studies on the basis of good protein expression in HEK293S GnTI $^-$ cells (ATCC, not tested for mycoplasma contamination), the ability to catalyse mitochondrial calcium uptake when co-expressed with EMRE, and good biochemical stability in detergent-containing solutions. The cDNA of

zebrafish MCU (UniProt accession zgc:153607, synthesized by Synbio Tech Inc.) was ligated into the XhoI–EcoRI restriction sites of a BacMam expression vector[39], encoding the full-length protein followed by a C-terminal 1D4 tag (TETSQVAPA) that is recognized by the Rho-1D4 monoclonal antibody[40]. The resulting plasmid was transformed to DH10Bac *E. coli* competent cells to generate bacmid. Recombinant P1 baculoviruses were generated in Sf9 cells (Invitrogen, not tested for mycoplasma contamination) cultured in sf-900 III SFM medium (GIBCO) using cellfectin II reagents (Invitrogen). For protein expression, 100 mL P3 virus was used to infect 1 L culture of HEK293S GnTI $^{-}$ cells (.0–3.5 × 10^6 cells/mL) in Freestyle 293 media (GIBCO) supplemented with 2% FBS (GIBCO, catalogue A31606–02). After infection, the cells were incubated at 37 °C for 16 h, and then 5 mM sodium butyrate (Sigma-Aldrich) was added to the cell culture and cells were cultured at 30 °C for another 72 h before harvest.

2 L of cell pellet was resuspended in 100 mL lysis buffer (40 mM HEPES pH 7.4 150 mM NaCl, 5 μM $CaCl_2$, 0.15 mg/ml DNase I, 1.5μg/ml Leupeptin, 1.5μg/ml Pepstatin A, 1 mM AEBSF, 1 mM Benzamidine, 1 mM PMSF and 1:500 dilution of Aprotinin), and then solubilized by adding lauryl maltose neopentyl glycol (LMNG, Anatrace, from a 10% stock in water) to a final concentration of 1% and stirred at 4 °C for 1.5 h. Detergent-solubilized material was separated from the insoluble fraction by centrifugation at 43,000*g* for 1 h and the supernatant was filtered through a 0.22-μm polystyrene membrane (Millipore). Rho-1D4 monoclonal antibody was coupled to CNBR-activated Sepharose beads (GE healthcare) according to the manufacturer's protocol. 5 mL Rho-1D4 monoclonal antibody beads were added to the sample and rotated at 4 °C for 2 h. The beads were washed with 100 mL of buffer A (20 mM HEPES pH 7.4 150 mM NaCl, 5 μM $CaCl_2$, 0.5 mM digitonin and 0.01 mg/ml 18:1 cardiolipin). Zebrafish MCU protein was eluted by incubating with 2 mg/ml 1D4 peptide (TETSQVAPA, synthesized by Peptide 2.0) overnight at 4 °C, and further purified by size-exclusion chromatography on a Superose 6 increase, 10/300 GL column (GE Healthcare) equilibrated with buffer B (20 mM Tris(hydroxymethyl)-aminomethane (Tris) pH 8.5, 150 mM NaCl, 5 μM $CaCl_2$, 0.5 mM digitonin, 0.01 mg/ml cardiolipin and 0.4 mM Tris(2-carboxyethyl)phosphine). The peak fractions were pooled, concentrated to 5 mg/ml using a 100 kDa concentrator (Vivaspin-2), and immediately used for cryo-EM grid preparation.

EM sample preparation and data acquisition

5 μL of 5 mg/mL freshly purified CeMCU and zebrafish MCU protein samples were loaded into glow-discharged (10 s) Quantifoil R1.2/1.3 holey carbon grids (Au 400, Electron Microscopy Sciences) and plunge-frozen in liquid nitrogen-cooled liquid ethane, using a Vitrobot Mark IV (FEI) operated at room temperature with a blotting time of 2 s under blot force of 0 at 100% humidity. Grids were clipped and loaded into a 300 keV Titan Krios microscope (FEI) equipped with a Gatan K2 Summit direct electron detector (Gatan). Grids were screened first for quality control based on the particle distribution and density, and images from the best grids were recorded. The CeMCU micrographs were collected at a magnification of 29,000 × with a super-resolution pixel size of 0.4307 Å and a defocus range of −0.9 to −2.9 μm. The dose rate was 8 electrons per physical pixel per second, and images were recorded for 8 s with 0.2 s subframes (40 total frames) corresponding to a total dose of

approximately 80 electrons per Å^2. The micrographs for zebrafish MCU were collected at a magnification of 37,000 × with a super-resolution pixel size of 0.346 Å and a defocus range of −1.2 to −3.2 μm. The dose rate was 8 electrons per physical pixel per second and images were recorded for 6 s with 0.13 s subframes (46 total frames) corresponding to a total dose of approximately 100 electrons per Å^2.

Image processing of CeMCU

Extended Data Figure 3 shows the cryo-EM workflow of CeMCU. Movie stacks were gain-corrected and twofold Fourier cropped to a calibrated pixel size of 0.8613 Å, and motion corrected and dose weighted using MotionCor2[41]. Contrast Transfer Function (CTF) estimates for motion-corrected micrographs were performed in CTFFIND4 using frames 1–40[42]. Subsequent image processing was carried out with RELION 2.1[43], using a particle box size of 384 pixels and a mask diameter of 160 Å, unless stated otherwise. The initial data set (~3700 movies) was obtained from two equivalent data collection sessions. Each micrograph was inspected manually; poor-quality ones and those having CTF estimation fits to lower than 5 Å were discarded. Approximately 2000 particles were picked manually and these were used for reference-free 2D classification to generate templates for automatic particle picking. Auto-picking (using 8 of the representative 2D classes containing different orientations as templates) from ~3,700 micrographs yielded 240,516 particles, which were further cleaned-up by removing outlier particles using two rounds of reference-free 2D classification with 100 classes (for example, to remove contaminants or empty micelles), and resulted in 201,281 particles. An initial 3D model from these particles was generated without imposed symmetry (C1 symmetry) with RELION 2.1. Using this initial model, 3D classification with C1 symmetry was performed, sorting the particles into 10 classes. The 10 classes had similar shapes and all indicated a tetrameric architecture. By visual inspection in UCSF Chimera[44], 8 “good” classes (representing 171,407 particles) were combined and subjected to 3D refinement. This yielded a reconstruction at 4.8 Å overall resolution in C1 symmetry. “Polished” particle images, which are corrected for individual particle movements, were generated in Relion using aligned movie frames that were output from MotionCor2. 3D refinement using the 171,407 polished particles and a mask that removes the micelle region yielded a reconstruction to 4.5 Å overall resolution with C1 symmetry. Well-defined density for α-helices enabled determination of the appropriate hand for the reconstruction at this point (Extended Data Fig. 3). The C2 overall symmetry of the molecule was evident from this map: it has fourfold symmetry within the TMD and twofold symmetry within the matrix region (Fig. 1a). Refinement using C2 symmetry in RELION 2.1 improved the overall resolution to 4.1 Å. All resolution estimates are based on gold-standard Fourier shell correlation (FSC) calculations.

To improve the reconstruction further, an additional ~2340 micrographs were collected using the same microscope and the same data collection strategy. These were motion-corrected using MotionCor2 as indicated above. Auto-picked particles were subjected to one round of reference-free 2D classification and merged with the previous data set at the “un-polished” stage to yield a total of 547,637 particles. 3D refinement in RELION 2.1 was performed using all of these particles (with C2 symmetry) and the particles were “polished” together as a single data set using methods described above. The polished particles were then subjected

to 3D classification, with C2 symmetry, sorting them into 10 classes. 8 good classes containing 376,541 polished particles were combined and subjected to 3D refinement in RELION 2.1 but this did not improve the overall resolution beyond 4.1 Å. All of these particles were imported into the cisTEM cryo-EM software package for further refinement[45]. 3D refinement in cisTEM, using the previously used mask, but where the micelle region outside the mask was low-pass filtered at 15 Å rather than removed, yielded the final reconstruction at 3.2 Å overall resolution. We suspect that this low-pass filter and the weighting scheme used for reconstruction in cisTEM were the primary reasons for the improved resolution[45]. The map was B-factor sharpened using a B-factor of −90 $Å^2$ and low-pass filtered at 3.2 Å resolution (using cisTEM). Independent half-maps were generated and only one of them was used to build and refine the atomic model; the other was used only for validation. We note that the additional data set was important to extend the resolution of the reconstruction; refinement in cisTEM using only the initial 171,407 polished particles yielded a reconstruction to 3.8 Å overall resolution. Estimation of the local resolution of the map was done using blocres[46]. The maps of CeMCU shown in Figures are combined maps, which were sharpened (using a *B*-factor of −90 $Å^2$) and low-pass filtered at 3.2 Å using cisTEM.

Model building and refinement

The atomic model of CeMCU was manually built into one of the half-maps (sharpened using a B-factor of −90 $Å^2$ and low-pass filtered at 3.2 Å resolution) and refined in real space using the COOT software[47]. The crystal structure of the NTD from human MCU (PDB: 5KUI) was used as a reference for the corresponding regions. Further refinement of the atomic model was carried out in PHENIX[48] using real-space refinement against the same half-map. The final model has good stereochemistry and good Fourier shell correlation with the other half-map as well as the combined map (Extended Data Fig. 6e and Extended Data Table 1). Structural Figures were prepared with Pymol (pymol.org), Chimera[44], and HOLE[49]. Electrostatic calculations used the APBS[50] plugin in Pymol.

Image processing of zebrafish MCU

Extended Data Figure 4 shows the cryo-EM workflow for zebrafish MCU. Movie stacks were gain-corrected, twofold Fourier cropped to a calibrated pixel size of 0.692 Å, motion corrected, and dose weighted using MotionCor2[3]. Contrast transfer function (CTF) estimates were performed in CTFFIND4 using frames 1–46[4]. Subsequent image processing was carried out in RELION 2.1[5]. Generating an improved initial model was crucial for 3D refinement of zebrafish MCU (Extended Data Fig. 4a). The improved initial model was generated using a subset of particles but refinement (Extended Data Fig. 4b) was done using the majority of particles as described below. Approximately 3000 particles were manually picked and subjected to 2D classification. Nine 2D-class averages were selected as templates for autopicking of 269,574 particles from ~3500 micrographs in RELION 2.1. After 2D classification to remove a few bad classes, 203,213 particles were used for ab-initio 3D model generation (with 4 classes) in cryoSPARC[6]. The best 3D reconstruction and the associated particle images were used for further 3D classification in RELION 2.1, sorting the particles into 6 classes. Three “good” classes (91,727 particles) were combined and subjected to further 3D classification (using 6 classes). The best class (representing 15,775

particles) was improved by 3D refinement in RELION 2.1 and yielded the improved initial model (Extended Data Fig. 4a). At this point, particles from micrographs with CTF fits better than 5 Å were selected (196,272 particles) and used for homogeneous refinement in cryoSPARC using the improved initial model (Extended Data Fig. 4b). This yielded a reconstruction at 9.1 Å overall resolution. All 196,272 particles were imported into cisTEM for further refinement[8]. 3D refinement in cisTEM, using a mask to apply a 30 Å low-pass filter to the detergent micelle, improved the overall resolution to 8.5 Å. The map shown in Figure 2 was B-factor sharpened using a B-factor of −90 $Å^2$ and low-pass filtered at 8.5 Å resolution (using cisTEM).

Cross-linking

For cross-linking of purified CeMCU in detergent, the protein was diluted to 0.2 mg/mL in buffer consisting of 20 mM HEPES, pH7.5, 150 mM NaCl, 1 mM $CaCl_2$, 1 mM DDM and 0.05 mg/mL cardiolipin. O to 1 mM concentrations of bis(sulfosuccinimidyl) suberate crosslinker (BS-3, Sigma-Aldrich, from a 17.5 mM stock in water) were added and the samples were incubated for 30 min at room temperature. The reactions were stopped by the addition of 140 mM Tris, pH 8.5, and analysed by 4–12% SDS-polyacrylamide gel electrophoresis under reducing conditions (100 mM dithiothreitol) using coomassie staining. For cross-linking of purified zebrafish MCU in detergent, the protein was diluted to 0.5 mg/mL in buffer consisting of 20 mM HEPES, pH7.5, 150 mM NaCl, 1 mM $CaCl_2$, 0.5 mM digitonin and 0.01 mg/mL cardiolipin. O to 1 mM concentrations of BS-3 crosslinker were added and the samples were incubated for 60 min on ice. The reactions were stopped by the addition of 100 mM Tris, pH 8.5, and analysed by 12% SDS-polyacrylamide gel electrophoresis under reducing conditions (100 mM dithiothreitol) using coomassie staining.

For cross-linking of human (Hs) MCU in MCU/EMRE knockout cell membranes, a chimaeric protein, consisting of the mitochondrial targeting sequence from *D. discoideum* MCU, fused to the mature form of human MCU (DdMTS–HsMCU) as previously used[16], followed by cDNA encoding a C-terminal Rho-1D4 affinity tag (amino acids: TETSQVAPA) and a stop codon, was cloned into the XhoI–EcoRI restriction sites of expression vector pCGFP-EU[36], transfected into MCU/EMRE knockout cells using Lipofectamine 3000 (Invitrogen), and the cells were cultured for 48 h at 37 °C with 5% CO_2. Cells were harvested and re-suspended in a buffer containing 50 mM HEPES, pH 7.5, 200 mM NaCl, 1 mM $CaCl_2$ and 1:500 dilution of Protease Inhibitor Cocktail III, EDTA-free (CalBiochem), and lysed by dounce homogenization and brief sonication (30 s) using a bath sonicator. Cell debris was removed by centrifugation (2500*g*, 4 °C, 15 min) and the membrane fractions were collected by centrifugation (100,000*g*, 4 °C, 1 h). The membrane fraction pellets were re-suspended in the same buffer using a dounce homogenizer followed by brief sonication (30 s), and treated with 0–575 μM of membrane permeable crosslinker disuccinimidyl glutarate (DSG, Pierce, from a 30 mM stock in DMSO) for 30 min at room temperature. The reactions were stopped by the addition of 140 mM Tris, pH 8.5, run on a 4–12% SDS-polyacrylamide gel under the reducing conditions (100 mM dithiothreitol), and detected by western blot using the Rho-1D4 antibody[40].

Generation of MCU/EMRE knockout HEK293T cells

SMDT1 and *MCU*, which encode human EMRE and MCU, respectively, were simultaneously targeted in HEK293T cells (Invitrogen, not tested for mycoplasma contamination) following a well-established CRISPR–Cas9 protocol[51]. In brief, sgRNA sequences targeting coding regions of *SMDT1* and *MCU* were selected using an online design tool (http://crispr.mit.edu/). Oligonucleotides incorporating target sequences for *SMDT1* (`5′-caccgATGGCGATGTCTCCGCCGCA-3′`, `5′-aaacTGCGGCGGAGACATCGCCATc-3′`) and *MCU* (`5′-caccgTGACAGCGTTCACGCCGGGA-3′`, `5′-aaacTCCCGGCGTGAACGCTGTCAc-3′`) were synthesized by IDT, annealed and cloned into the pSpCas9(BB)-2A-GFP vector (Addgene plasmid # 48138). Correctly inserted sgRNA sequences were verified for the *SMDT1*- and *MCU*-targeting vectors by Sanger sequencing (Genewiz). HEK293T cells (Thermo Fisher) were detached with trypsin and seeded into a 24-well plate with approximately 1.3×10^5 cells per well. Twenty-four hours after seeding, cells were transfected with 0.25 μg of each vector using Lipofectamine2000 (Invitrogen). Twenty-four hours post-transfection, cells were detached and single GFP-positive cells were sorted into individual wells of a 96-well plate containing DMEM (supplemented with 20% FBS, 100 U/ml penicillin, and 100 μg/ml streptomycin) using a BD FACSAria II cell sorter. After sorting, cells were incubated for 2 weeks, during which time media was changed every 3–5 days, and wells were monitored for the appearance of well-defined single colonies. Colonies were then transferred to a 24-well plate for subsequent outgrowth, DNA analysis, and functional characterization. Genomic DNA from individual colonies was prepared using QuickExtract solution according to the manufacturer's instructions. Loci containing the targeted sequences were PCR amplified and Sanger sequenced using the following primers: `5′-TAACGAATTCCACAGATAGCACGGGCCTTT-3′`, `5′-TATGGTCGACTAGCGTATTCTTGGTCCGCC-3′` for *SMDT1* and `5′-TAACGAATTCACCCCCATGCAAGAATGGTA-3′`, `5′-TATGGTCGACGTTCATCCTTGCTCATGGCATT-3′` for *MCU*. Putative double knockouts that were disrupted at both *SMDT1* and *MCU* loci (as judged by Sanger sequencing) were verified functionally using the mitochondrial Ca^{2+} uptake assay.

Mitochondrial Ca^{2+} uptake measurements

The cDNA for zebrafish MCU, zebrafish $MCU_{\Delta NTD}$ (deletion from residue 85 to residue 190), zebrafish EMRE (UniProt accession: Q08BI9), DdMTS–HsMCU chimaera, and human EMRE (UniProt accession: Q9H4I9) were sub-cloned into the pCGFP-EU mammalian expression vector with a C-terminal 1D4 tag (and without GFP)[36]. Mutations were generated using Q5 Site-Directed Mutagenesis Kit (New England BioLabs Inc.) and verified by DNA sequencing.

1.5 μg MCU plasmid and 1.5 μg EMRE plasmid were co-transfected into ~2×10^6 MCU/EMRE knockout cells using Lipofectamine2000 (Invitrogen). After transfection, the cells were cultured at 37 °C for ~48 h and then collected for calcium uptake assays and western blotting.

Calcium uptake assays of permeabilized MCU/EMRE knockout cells were performed according to a published protocol[16]. In brief, ~2×10^6 cells were resuspended in 1 mL of

buffer containing 125 mM KCl, 2 mM K_2HPO_4, 1 mM $MgCl_2$, 10 μM ethylene glycol-bis(2-aminoethylether)-*N,N,N′,N′*-tetraacetic acid (EGTA, Gold Biotechnology), 5 mM malate, 5 mM glutamate, 5 mM succinate (Sigma-Aldrich) and 20 mM HEPES, pH 7.4, and loaded into a stirred quartz cuvette in a Hitachi F-2500 spectrophotometer (excitation: 506 nm, slit length: 3 nm, emission: 531 nm, slit length: 3 nm, sampling frequency: 2 Hz), with the temperature maintained at 22 °C by a circulating bath. In a typical experiment, reagents were added into the cuvette in the following order: 1 μM cell-impermeable Calcium Green-5N (Life Technologies, from a 1 mM stock solution in water), 0.005% (w/v) digitonin (Sigma-Aldrich, from a 0.5% stock solution in water), 5 μM $CaCl_2$, and either 1 μM ruthenium red (Sigma-Aldrich, from a 0.2 mM stock solution in water), 5 μM carbonyl cyanide *m*-chlorophenyl hydrazone (CCCP, Sigma-Aldrich, from a 1 mM stock solution in DMSO) or 10 μM ETH129 (Calcium ionophore II, Sigma-Aldrich, from a 2 mM stock solution in DMSO). For the data plotted in Figure 4d, a rate of Ca^{2+} uptake was defined as the slope of a linear fit of the Ca^{2+} uptake curve between 240 and 260 s (for example, Extended Data Fig. 2d, f). Relative uptake (Fig. 4d) is the ratio of the slopes observed for mutant and wild type MCU channels.

Extended Data

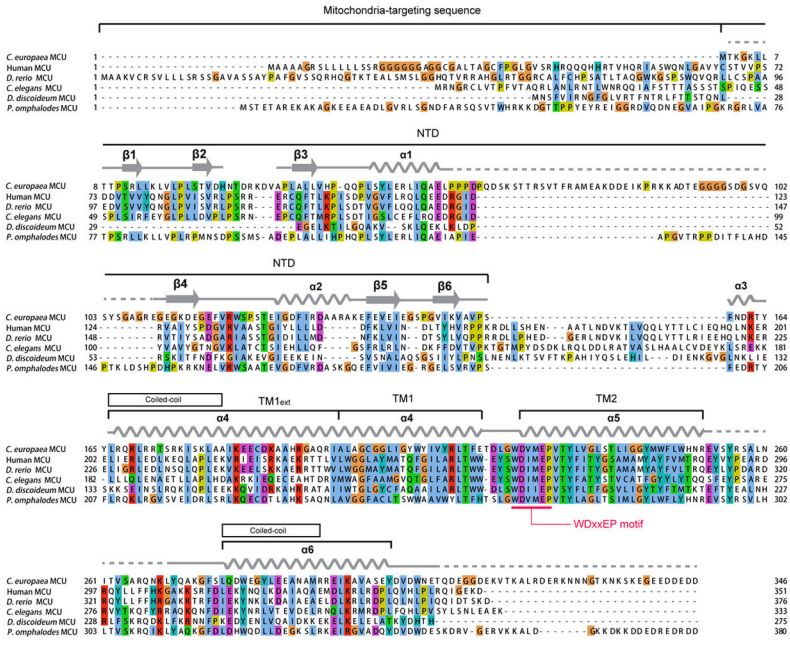

Extended Data Fig. 1 |. Structure-based sequence alignment.

The amino acid sequences of the *C. europaea*, *Pyronema omphalodes*, *D. discoideum*, *C. elegans*, zebrafish (*D. rerio*) and human MCU are aligned and coloured according to the ClustalW convention (UniProt accession numbers: W2SDE2, U4LFM6, Q54LT0, Q21121, Q08BI9 and Q8NE86, respectively). The secondary structure is indicated with ribbons representing α-helices, solid lines representing structured loop regions, and dashed lines representing disordered regions. The WDXXEP signature sequence is highlighted with a red line. The amino acids drawn as sticks in Fig. 5c that face the vestibule are: Ile198, Ala199, Gly202, Leu206 and Tyr209 from TM1 and Tyr232, Gly235, Leu236, Thr238, Leu239,

Tyr243, and Phe246 from TM2; the corresponding amino acids in human MCU are: Val235, Leu236, Gly239, Met243, Gln246, Tyr268, Thr271, Tyr272, Ser274, Ala275, Tyr279 and Phe282, respectively. Basic residues at the matrix boundary of the membrane (for example, Arg193, Arg197, and Arg251 of CeMCU) may interact with phospholipid headgroups.

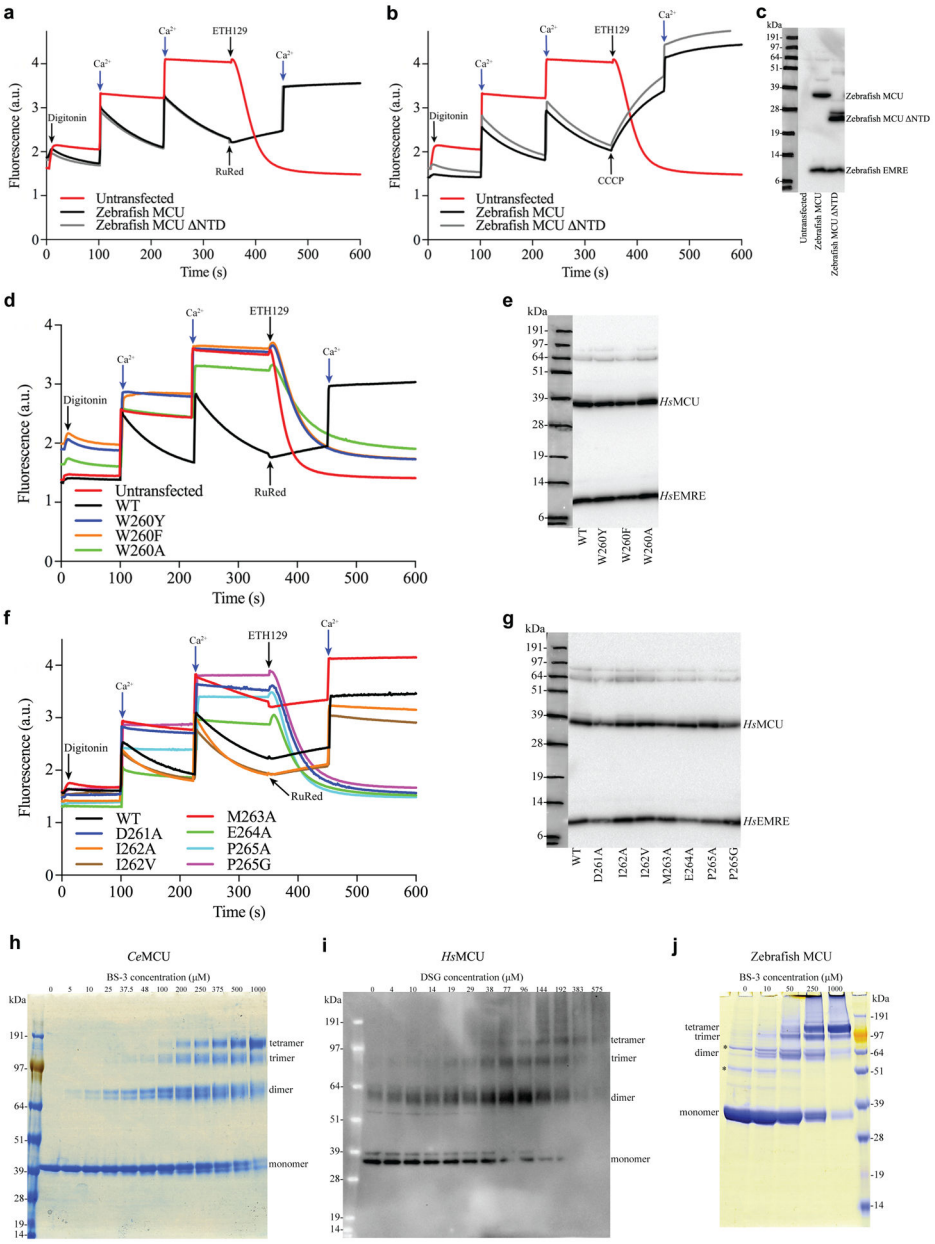

Extended Data Fig. 2 |. Functional analysis of MCU.

a, **b**, Representative Ca^{2+} uptake experiments using digitonin-permeabilized MCU/EMRE knockout cells without transfection (red line), or expressing zebrafish MCU and EMRE (black line), or expressing zebrafish $MCU_{\Delta NTD}$ and EMRE (grey line). Blue arrows indicate additions of 5 μM $CaCl_2$. A decrease in fluorescence following addition of Ca^{2+} is indicative of Ca^{2+} uptake (for example, black and grey traces). Ruthenium red (RuRed), a proton

ionophore (CCCP), or a Ca^{2+} ionophore (ETH129) were added as controls towards the end of each experiment as indicated. RuRed prevents Ca^{2+} uptake, ETH129 demonstrates that the mitochondria are intact, and CCCP demonstrates that Ca^{2+} uptake is dependent upon the proton gradient. Analogous experiments were repeated six times with similar results. **c**, Rho-1D4 western blot analysis of the cell lysates from **a**, demonstrating expression of MCU and EMRE, which were C-terminally tagged with a 1D4 peptide (see Methods). Repeated twice with similar results. **d**, **f**, Representative mitochondrial Ca^{2+} uptake experiments using MCU/EMRE knockout cells for the indicated mutations of human MCU when co-transfected with EMRE (from which the data shown in Fig. 4d are derived, see Methods). Independent experiments were repeated with similar results: $n = 8$ for wild type, $n = 9$ for M263A, and $n = 3$ for the remainder of the mutants. **e**, **g**, Full-size western blots of the cell lysates from **d** and **f** showing protein expression levels (corresponding to Fig. 4d; detected using a Rho-1D4 antibody). Repeated twice with similar results. **h**, **i**, Subunit stoichiometry analysis of MCU proteins using crosslinking. **h**, Crosslinking of purified CeMCU in the detergent *n*-dodecyl-β-D-maltoside (DDM). Indicated concentrations of the crosslinker bis(sulfosuccinimidyl) suberate (BS-3) were incubated with purified CeMCU. Analysis is by SDS–PAGE and coomassie stain. Molecular weight standards are located in the first lane and their positions indicated. The calculated molecular weight of CeMCU is 39.6 kDa based upon its amino acid sequence. Repeated three times with similar results. **i**, Crosslinking of HsMCU expressed in HEK293 membranes. Indicated concentrations of the membrane-permeable crosslinker disuccinimidyl glutarate (DSG) were used and HsMCU was detected by western blot using a C-terminal Rho-1D4 antibody tag (Methods). Molecular weight standards are located in the first lane and their positions indicated. We note that some oligomerization of human MCU was observed without crosslinker; this phenomenon has been observed previously for human MCU[32]. Repeated four times with similar results. **j**, Crosslinking of purified zebrafish MCU in the detergent digitonin. Indicated concentrations of BS-3 crosslinker were used. Samples were analysed by SDS–PAGE using coomassie stain. Molecular weight standards are located in the last lane and their positions are indicated. Asterisks indicate protein impurities. Repeated twice with similar results.

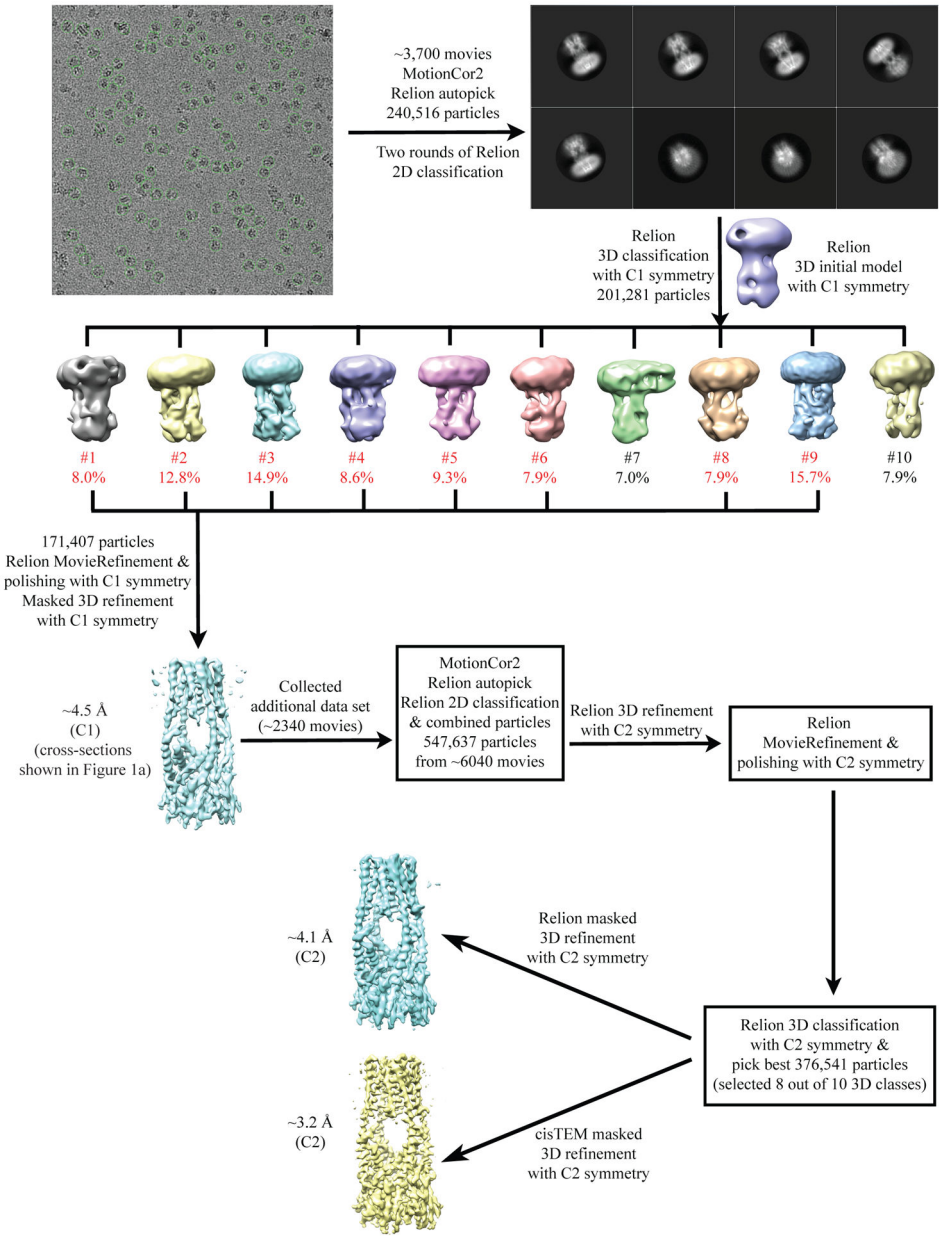

Extended Data Fig. 3 |. Flowchart for cryo-EM data processing of CeMCU.
Details can be found in the Methods.

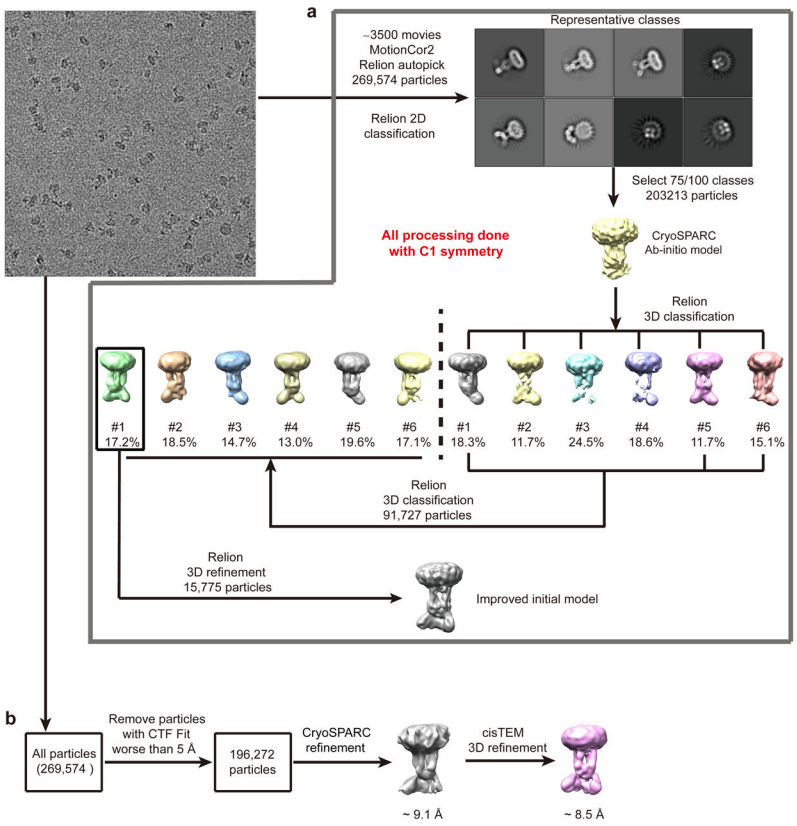

Extended Data Fig. 4 |. Flowchart for cryo-EM data processing of zebrafish MCU.

a, Initial model generation and improvement. **b**, 3D refinement using the improved initial model from **a**. Details can be found in the Methods.

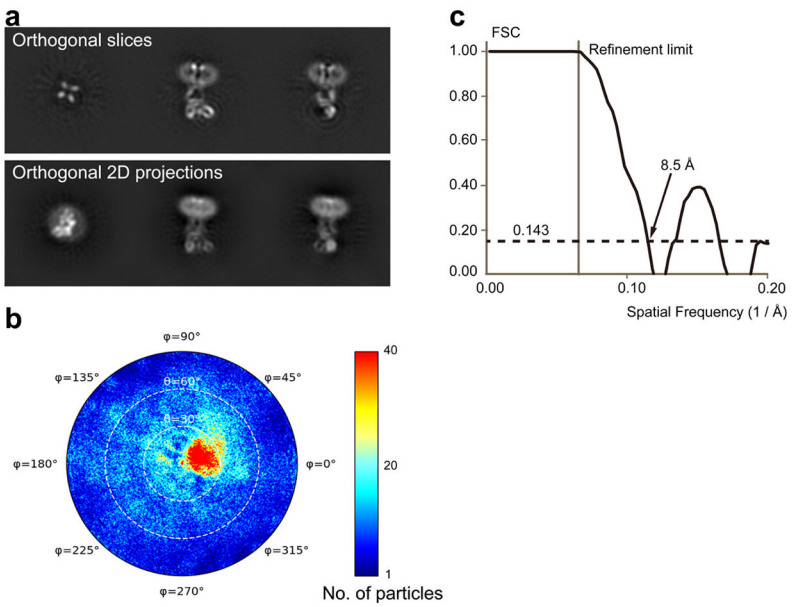

Extended Data Fig. 5 |. Cryo-EM reconstruction of zebrafish MCU.

a, Orthogonal slices (top) and orthogonal 2D projections (bottom) of the final 3D reconstruction (from cisTEM). **b**, Angular orientation distribution of the particles used in the final reconstruction. The particle distribution is indicated by different colour shades. **c**, Gold-standard FSC curve of the final 3D reconstruction. The resolution is ~8.5 Å at the FSC cutoff of 0.143. A thin vertical line indicates that only spatial frequencies to 1/(15 Å) were used to determine particle alignment parameters during refinement in cisTEM.

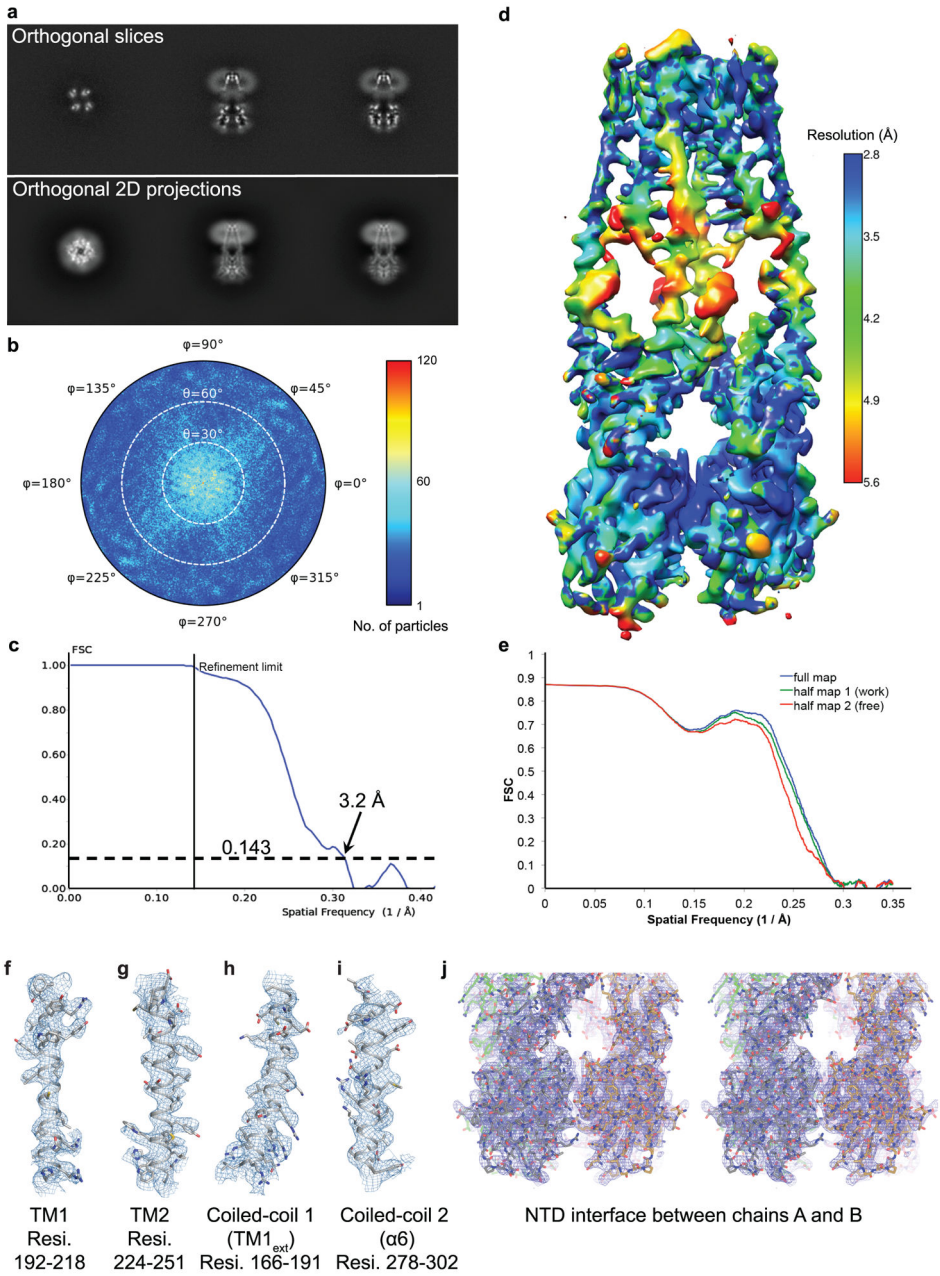

Extended Data Fig. 6 |. Cryo-EM structure determination and density of CeMCU.
a, Orthogonal slices (top) and orthogonal 2D projections (bottom) of the final 3D reconstruction (from cisTEM). **b**, Angular orientation distribution of the particles used in

final reconstruction. The particle distribution is indicated by different colour shades. **c**, Gold-standard FSC curve of the final 3D reconstruction. The resolution is ~3.2 Å at the FSC cutoff of 0.143. A thin vertical line indicates that only spatial frequencies to 1/(7 Å) were used to determine particle alignment parameters during refinement. **d**, Local resolution of the map estimated using the blocres program and coloured as indicated. **e**, Model validation. Comparison of the FSC curves between model and half map 1 (work), model and half map 2 (free), and model and full map are plotted in green, red and blue, respectively. **f**–**i**, Densities (8σ contours) of α-helical regions of CeMCU are shown in the context of the atomic model with side chains shown as sticks and the backbone as ribbons. **j**, Stereo representation of the density (8σ contour) of the NTDs, with the interface between chains A and B in the foreground.

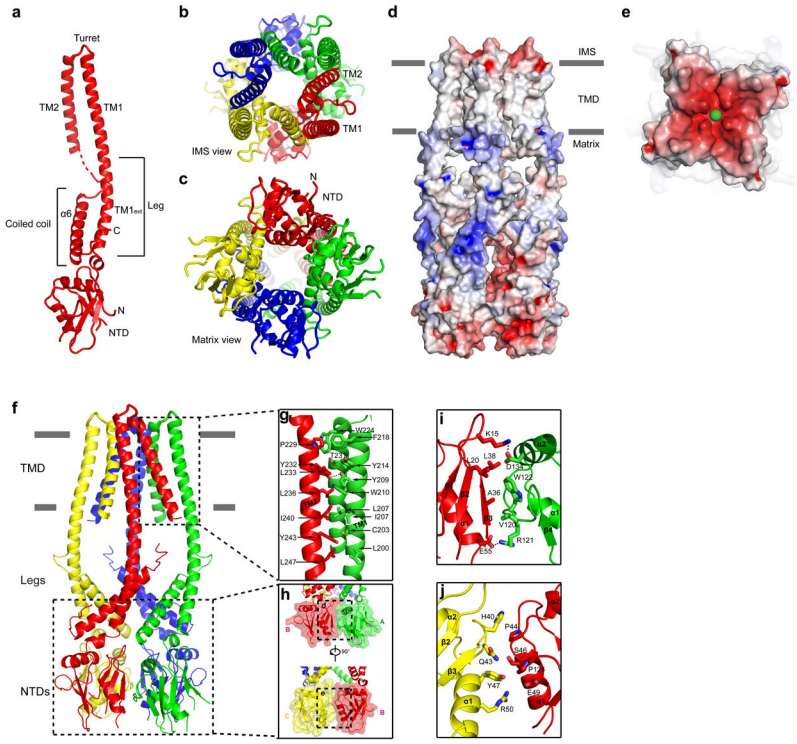

Extended Data Fig. 7 |. Structure of CeMCU.

a, Ribbon representation of an isolated subunit from Fig. 1c, viewed parallel to the membrane, with the structural features labelled. Disordered regions connecting TM2 and α6 are indicated as dashed lines. **b**, **c**, IMS and matrix views of Fig. 1c. **d**, **e**, Molecular surface coloured according to electrostatic potential (red, −8 kT e^{-1}; white, neutral; blue, +8 kT e^{-1}). **d**, Shown in the same orientation as Fig. 1c with approximate membrane boundaries as grey bars. **e**, IMS view. A green sphere indicates the position of Ca^{2+} in site 1. **f**, Overall structure of CeMCU, depicted similarly to Fig. 1. **g**, Subunit interactions within the TMD. Ribbon representations of TM1 and TM2 from one subunit (green) and TM2 of the neighbouring subunit (red) are shown. Residues participating in van der Waals or hydrogen bonding interactions are shown as sticks; dashed lines indicate hydrogen bonds. Atom colouring: nitrogen, blue; oxygen, red; and sulfur, green. **h**, Interfaces within the NTDs. The

NTDs of subunit A, B and C (green, red and yellow, respectively) are shown in ribbon and surface representations. Each NTD contains six β-strands (β1 through β6) and two α-helices (α1 and α2). There are four interfaces between the NTDs, and these are of two types. Interface 1 (for example, between protomers A and B or C and D in the atomic model) consists of an interaction between β3 of one NTD and the β1–β2 loop of another; this interface buries 2,188 $Å^2$ of molecular surface in the assembled channel. Interface 2 (for example, between protomers A and D or B and C) is less extensive, burying 1,440 $Å^2$ total surface area, and involves contacts located near the N-terminal ends of the α1 helices from two NTDs. **i**, **j**, Details of interfaces 1 and 2 between NTDs, respectively.

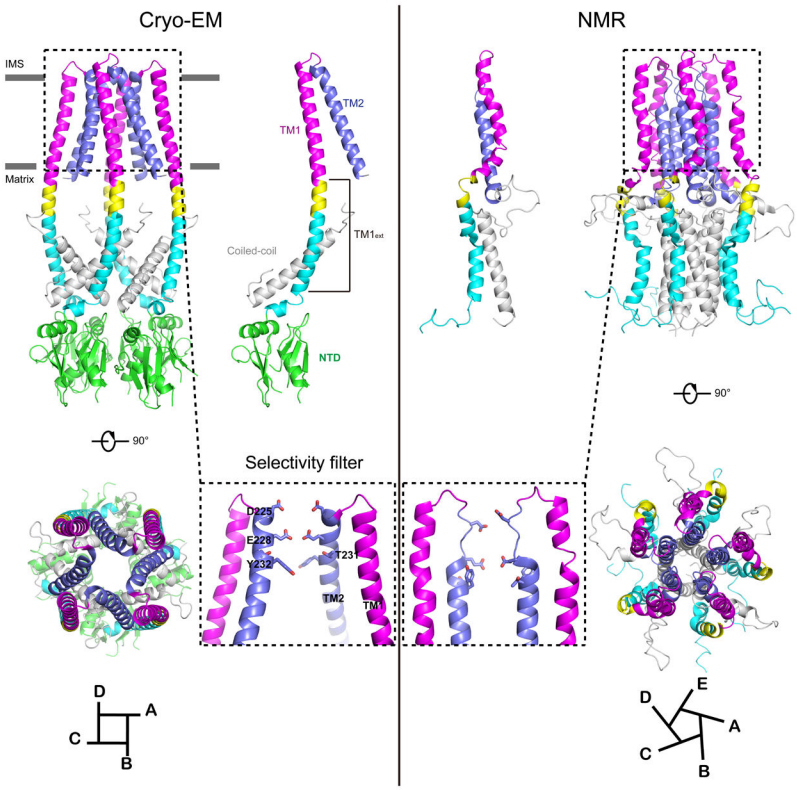

Extended Data Fig. 8 |. Comparison with an NMR structure (PDB: 5ID3).
Left, various representations of the cryo-EM structure of CeMCU. The NTD, $TM1_{ext}$, TM1, TM2 and coiled-coil regions are shown in different colours. Right, structure deduced from NMR studies of *C. elegans* MCU-ΔNTD (PDB: 5ID3). It is coloured according to the cryo-EM structure using the sequence alignment shown in Extended Data Fig. 1. The boxed regions highlight differences in vicinity of the WDXXEP signature sequence and pore. Pore-lining residues (D225, E228, T231 and Y232; *C. europaea* numbering) are shown as sticks.

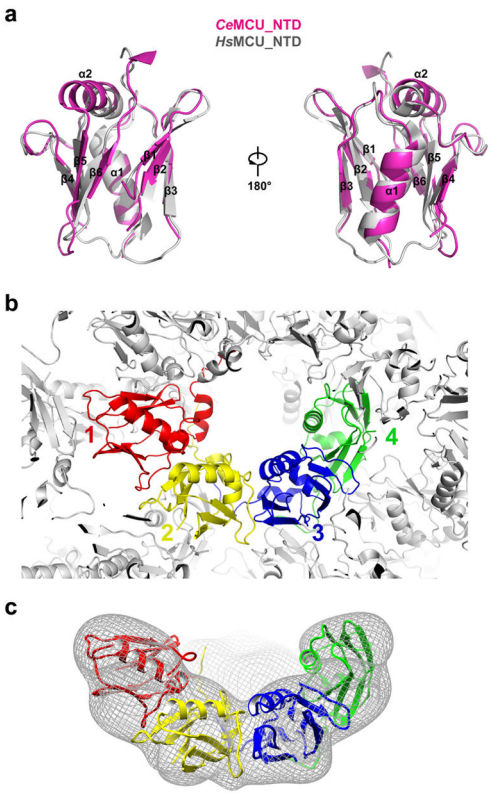

Extended Data Fig. 9 |. Structural comparison of the NTDs of CeMCU, zebrafish MCU and human MCU.

a, An NTD from the cryo-EM structure of CeMCU (red) is superimposed with the crystal structure of an isolated NTD from human MCU (grey, PDB: 5KUG, r.m.s.d. = 2.0 Å). The secondary structure features are indicated; two views are shown. **b**, Crystal lattice from an X-ray structure of an isolated NTD of human MCU (PDB: 4XTB). Four neighbouring NTDs are coloured and other NTDs are grey. A similar arrangement is present in PDB 5KUG. **c**. Matrix view of the cryo-EM reconstruction of zebrafish MCU (from Fig. 2d).

Extended Data Table 1 |

Cryo-EM data collection, refinement and validation statistics

	***Ce*MCU (EMD-7971) (PDB 6DNF)**	**Zebrafish MCU (EMDB-7972)**
Data collection and processing		
Microscope	FEI Titan Krios (at MSKCC)	FEI Titan Krios (at MSKCC)
Camera	Gatan K2 Summit	Gatan K2 Summit
Magnification	29,000×	37,000×
Voltage (kV)	300	300
Electron exposure (e^{-}/Å^2)	80	100.2
Defocus range (μm)	−0.9 ~ −2.9	−1.2 ~ −3.2
Pixel size (Å)	0.8613 (0.4307)*	0.692 (0.346)*

	***Ce*MCU (EMD-7971) (PDB 6DNF)**	**Zebrafish MCU (EMDB-7972)**
Software	RELION 2.1, cisTEM 1.0	RELION 2.1, cryoSPARC, cisTEM 1.0,
Symmetry imposed	C2	C1
Initial particle images (no.)	547,637	269,574
Final particle images (no.)	376,541	196,272
Overall map resolution (Å)	3.2	8.5
FSC threshold 0.143		
Local map resolution range (Å)	2.8–5.6	
Refinement		
Software	Phenix 1.13 real-space-refine	
Initial model used (PDB code)	N/A	
Model resolution (Å)	4.0	
FSC threshold 0.5		
Map sharpening *B* factor (Å^2)	−90	−90
Model composition		
Non-hydrogen atoms	7,312	
Protein residues	900	
Ligands	3	
Lipids	8	
B factors (Å^2)		
Protein	136.7	
Ligand	153.9	
R.m.s. deviations		
Bond lengths (Å)	0.016	
Bond angles (°)	0.830	
Validation		
MolProbity score	1.26	
Clashscore	1.82	
Poor rotamers (%)	0.0	
Ramachandran plot		
Favored (%)	95.4	
Allowed (%)	4.6	
Disallowed (%)	0.0	

Values in parentheses indicate the pixel size for super-resolution mode.

Acknowledgements

We thank N. Grigorieff, members of his laboratory, and the staff at the Howard Hughes Medical Institute Cryo-EM facility for training in cryo-EM; R. K. Hite and members of the Long laboratory for discussions; the staff of the New York Structural Biology Center Simons Electron Microscopy Center, M. Ebrahim, and M. J. de la Cruz of the Memorial Sloan Kettering Cancer Center Cryo-EM facility for help with data collection; and J. Goldberg for spectrophotometer use. This work was supported, in part, by an NIH core facilities grant to Memorial Sloan Kettering Cancer Center (P30 CA008748), by an NIH Medical Scientist Training Program grant (T32GM007739 for A.F.S.), and by an NIH grant (R01GM094273 to S.B.L.).

References

1. Deluca HF & Engstrom GW Calcium uptake by rat kidney mitochondria. Proc. Natl Acad. Sci. USA 47, 1744–1750 (1961). [PubMed: 13885269]
2. Montero M et al. Chromaffin-cell stimulation triggers fast millimolar mitochondrial Ca2+ transients that modulate secretion. Nat. Cell Biol 2, 57–61 (2000). [PubMed: 10655583]
3. Baughman JM et al. Integrative genomics identifies MCU as an essential component of the mitochondrial calcium uniporter. Nature 476, 341–345 (2011). [PubMed: 21685886]
4. De Stefani D, Raffaello A, Teardo E, Szabò I & Rizzuto R A forty-kilodalton protein of the inner membrane is the mitochondrial calcium uniporter. Nature 476, 336–340 (2011). [PubMed: 21685888]
5. Chaudhuri D, Sancak Y, Mootha VK & Clapham DE MCU encodes the pore conducting mitochondrial calcium currents. eLife 2, e00704 (2013). [PubMed: 23755363]
6. Kamer KJ & Mootha VK The molecular era of the mitochondrial calcium uniporter. Nat. Rev. Mol. Cell Biol 16, 545–553 (2015). [PubMed: 26285678]
7. Gunter KK & Gunter TE Transport of calcium by mitochondria. J. Bioenerg. Biomembr 26, 471–485 (1994). [PubMed: 7896763]
8. Kirichok Y, Krapivinsky G & Clapham DE The mitochondrial calcium uniporter is a highly selective ion channel. Nature 427, 360–364 (2004). [PubMed: 14737170]
9. Bick AG, Calvo SE & Mootha VK Evolutionary diversity of the mitochondrial calcium uniporter. Science 336, 886 (2012). [PubMed: 22605770]
10. Sancak Y et al. EMRE is an essential component of the mitochondrial calcium uniporter complex. Science 342, 1379–1382 (2013). [PubMed: 24231807]
11. Perocchi F et al. MICU1 encodes a mitochondrial EF hand protein required for Ca(2+) uptake. Nature 467, 291–296 (2010). [PubMed: 20693986]
12. Plovanich M et al. MICU2, a paralog of MICU1, resides within the mitochondrial uniporter complex to regulate calcium handling. PLoS One 8, e55785 (2013). [PubMed: 23409044]
13. Mallilankaraman K et al. MCUR1 is an essential component of mitochondrial Ca^{2+} uptake that regulates cellular metabolism. Nat. Cell Biol 14, 1336–1343 (2012). [PubMed: 23178883]
14. Vais H et al. MCUR1, CCDC90A, is a regulator of the mitochondrial calcium uniporter. Cell Metab. 22, 533–535 (2015). [PubMed: 26445506]
15. Chaudhuri D, Artiga DJ, Abiria SA & Clapham DE Mitochondrial calcium uniporter regulator 1 (MCUR1) regulates the calcium threshold for the mitochondrial permeability transition. Proc. Natl Acad. Sci. USA 113, E1872–E1880 (2016). [PubMed: 26976564]
16. Kovács-Bogdán E et al. Reconstitution of the mitochondrial calcium uniporter in yeast. Proc. Natl Acad. Sci. USA 111, 8985–8990 (2014). [PubMed: 24889638]
17. Tsai M-F et al. Dual functions of a small regulatory subunit in the mitochondrial calcium uniporter complex. eLife 5, e15545 (2016). [PubMed: 27099988]
18. Oxenoid K et al. Architecture of the mitochondrial calcium uniporter. Nature 533, 269–273 (2016). [PubMed: 27135929]
19. Moraes I, Evans G, Sanchez-Weatherby J, Newstead S & Stewart PD Membrane protein structure determination — the next generation. Biochim. Biophys. Acta 1838 (1 Pt A), 78–87 (2014). [PubMed: 23860256]
20. Long SB, Tao X, Campbell EB & MacKinnon R Atomic structure of a voltage-dependent K+ channel in a lipid membrane-like environment. Nature 450, 376–382 (2007). [PubMed: 18004376]
21. Payandeh J, Scheuer T, Zheng N & Catterall WA The crystal structure of a voltage-gated sodium channel. Nature 475, 353–358 (2011). [PubMed: 21743477]
22. Wu J et al. Structure of the voltage-gated calcium channel Cav1.1 complex. Science 350, aad2395 (2015). [PubMed: 26680202]
23. Shen H et al. Structure of a eukaryotic voltage-gated sodium channel at near-atomic resolution. Science 355, eaal4326 (2017). [PubMed: 28183995]
24. Yan Z et al. Structure of the rabbit ryanodine receptor RyR1 at near-atomic resolution. Nature 517, 50–55 (2015). [PubMed: 25517095]

25. Zalk R et al. Structure of a mammalian ryanodine receptor. Nature 517, 44–49 (2015). [PubMed: 25470061]
26. Fan G et al. Gating machinery of InsP3R channels revealed by electron cryomicroscopy. Nature 527, 336–341 (2015). [PubMed: 26458101]
27. Liao M, Cao E, Julius D & Cheng Y Structure of the TRPV1 ion channel determined by electron cryo-microscopy. Nature 504, 107–112 (2013). [PubMed: 24305160]
28. Hille B Ionic Channels of Excitable Membranes 3rd edn (Sinauer Associates, 2001). Sunderland, MA
29. Zhou Y, Morais-Cabral JH, Kaufman A & MacKinnon R Chemistry of ion coordination and hydration revealed by a K^+ channel–Fab complex at 2.0 A resolution. Nature 414, 43–48 (2001). [PubMed: 11689936]
30. Lee Y et al. Structure and function of the N-terminal domain of the human mitochondrial calcium uniporter. EMBO Rep. 16, 1318–1333 (2015). [PubMed: 26341627]
31. Lee SK et al. Structural insights into mitochondrial calcium uniporter regulation by divalent cations. Cell Chem. Biol 23, 1157–1169 (2016). [PubMed: 27569754]
32. Miller AN & Long SB Crystal structure of the human two-pore domain potassium channel K2P1. Science 335, 432–436 (2012). [PubMed: 22282804]
33. Brohawn SG, Campbell EB & MacKinnon R Physical mechanism for gating and mechanosensitivity of the human TRAAK K^+ channel. Nature 516, 126–130 (2014). [PubMed: 25471887]
34. Dong YY et al. K2P channel gating mechanisms revealed by structures of TREK-2 and a complex with Prozac. Science 347, 1256–1259 (2015). [PubMed: 25766236]
35. Doyle DA et al. The structure of the potassium channel: molecular basis of K^+ conduction and selectivity. Science 280, 69–77 (1998). [PubMed: 9525859]
36. Kawate T & Gouaux E Fluorescence-detection size-exclusion chromatography for precrystallization screening of integral membrane proteins. Structure 14, 673–681 (2006). [PubMed: 16615909]
37. Kilmartin JV, Wright B & Milstein C Rat monoclonal antitubulin antibodies derived by using a new nonsecreting rat cell line. J. Cell Biol 93, 576–582 (1982). [PubMed: 6811596]
38. Long SB, Campbell EB & Mackinnon R Crystal structure of a mammalian voltage-dependent Shaker family K^+ channel. Science 309, 897–903 (2005). [PubMed: 16002581]
39. Goehring A et al. Screening and large-scale expression of membrane proteins in mammalian cells for structural studies. Nat. Protocols 9, 2574–2585 (2014). [PubMed: 25299155]
40. Molday RS & MacKenzie D Monoclonal antibodies to rhodopsin: characterization, cross-reactivity, and application as structural probes. Biochemistry 22, 653–660 (1983). [PubMed: 6188482]
41. Zheng SQ et al. MotionCor2: anisotropic correction of beam-induced motion for improved cryo-electron microscopy. Nat. Methods 14, 331–332 (2017). [PubMed: 28250466]
42. Rohou A & Grigorieff N CTFFIND4: Fast and accurate defocus estimation from electron micrographs. J. Struct. Biol 192, 216–221 (2015). [PubMed: 26278980]
43. Fernandez-Leiro R & Scheres SHW A pipeline approach to single-particle processing in RELION. Acta Crystallogr. D Struct. Biol 73, 496–502 (2017). [PubMed: 28580911]
44. Pettersen EF et al. UCSF Chimera—a visualization system for exploratory research and analysis. J. Comput. Chem 25, 1605–1612 (2004). [PubMed: 15264254]
45. Grant T, Rohou A & Grigorieff N *cis*TEM, user-friendly software for single-particle image processing. eLife 7, e35383 (2018). [PubMed: 29513216]
46. Cardone G, Heymann JB & Steven AC One number does not fit all: mapping local variations in resolution in cryo-EM reconstructions. J. Struct. Biol 184, 226–236 (2013). [PubMed: 23954653]
47. Emsley P, Lohkamp B, Scott WG & Cowtan K Features and development of Coot. Acta Crystallogr. D Biol. Crystallogr 66, 486–501 (2010). [PubMed: 20383002]
48. Adams PD et al. PHENIX: a comprehensive Python-based system for macromolecular structure solution. Acta Crystallogr. D Biol. Crystallogr 66, 213–221 (2010). [PubMed: 20124702]

49. Smart OS, Neduvelil JG, Wang X, Wallace BA & Sansom MS HOLE: a program for the analysis of the pore dimensions of ion channel structural models. J. Mol. Graph. 14, 354–360 (1996). [PubMed: 9195488]

50. Baker NA, Sept D, Joseph S, Holst MJ & McCammon JA Electrostatics of nanosystems: application to microtubules and the ribosome. Proc. Natl Acad. Sci. USA 98, 10037–10041 (2001). [PubMed: 11517324]

51. Ran FA et al. Genome engineering using the CRISPR-Cas9 system. Nat. Protocols 8, 2281–2308 (2013). [PubMed: 24157548]

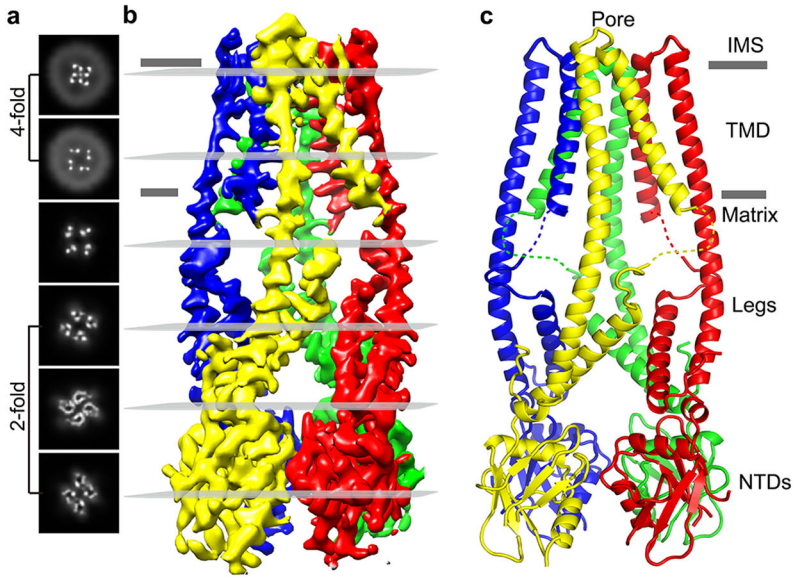

Fig. 1 |. Cryo-EM map and overall structure of CeMCU.

a, Slices of a 3D reconstruction generated without imposing symmetry (Extended Data Fig. 3). **b**, Final 3D reconstruction viewed parallel to the membrane (8σ contour level). Density for the detergent micelle is present at lower contours (for example, Extended Data Fig. 3). Subunits are coloured uniquely. **c**, Ribbon representation in the same orientation as **b**, with approximate membrane boundaries as grey bars. IMS, intermembrane space. Disordered regions connecting TM2 and α6 are indicated as dashed lines.

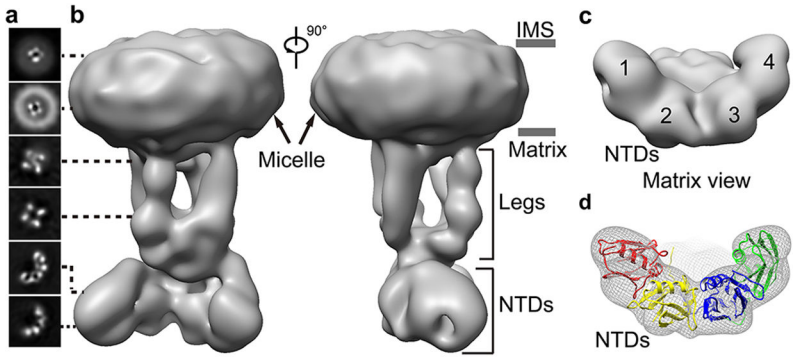

Fig. 2 |. Cryo-EM reconstruction of zebrafish MCU.

a, 2D slices of the 3D reconstruction of zebrafish MCU are shown at the indicated positions. **b**, Two orthogonal views of the 3D reconstruction viewed parallel to the membrane. Grey bars indicate approximate membrane boundaries. Density attributed to the detergent micelle surrounding the TMD is indicated. **c**, Matrix view, showing density for four NTDs. The TMD region is removed for clarity. **d**, Atomic models (PDB: 4XTB) of four NTDs are fit into the density from **c** (mesh).

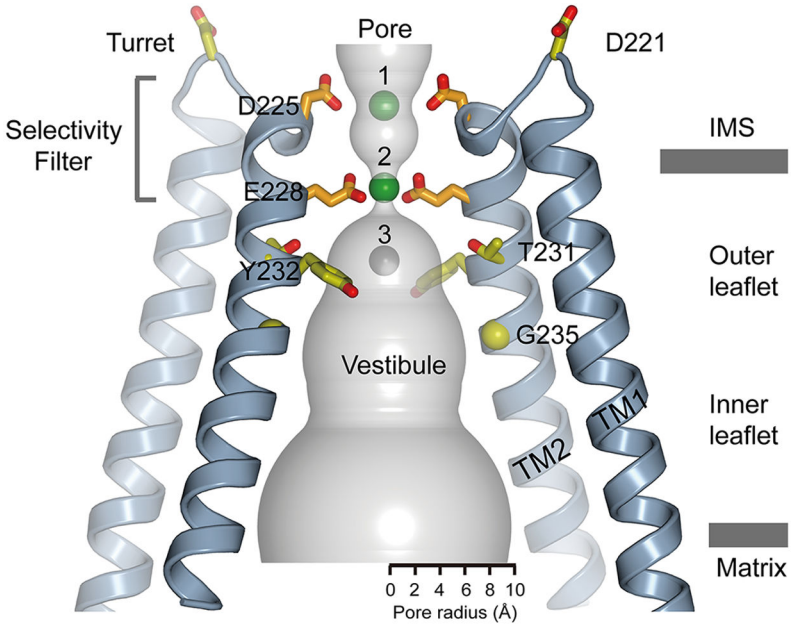

Fig. 3 |. Ion pore.

Within a ribbon representation of two subunits of CeMCU is a representation (grey surface) of the minimal radial distance from the centre of the pore to the nearest van der Waals protein contact. Selected amino acids are shown as sticks.

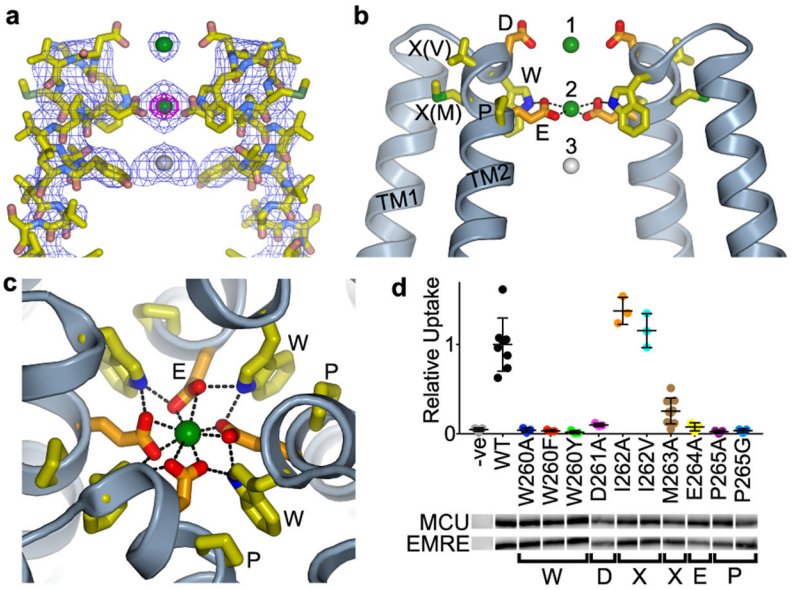

Fig. 4 |. Selectivity filter.

a, Density within the selectivity filter region of CeMCU. The map is contoured at 8σ (blue mesh) and 20σ (magenta mesh) and shown in the context of two TM2 helices (sticks; other regions are omitted for clarity). Green spheres indicate Ca^{2+} ions in sites 1 and 2; a grey sphere indicates site 3. **b**, Side view of the selectivity filter region, showing two subunits as ribbons and the WDXXEP signature sequence as sticks. Dashed lines indicate hydrogen bonds and Ca^{2+} coordination. **c**, Close up of site 2, oriented approximately 60° from the plane of the membrane, showing all four subunits. **d**, Mitochondrial Ca^{2+} uptake by indicated mutants of human MCU relative to wild type (WT) when co-expressed with EMRE (mean ± s.d., independent experiments: $n = 8$ for wild type, $n = 9$ for M263A, and $n = 3$ for the remainder, Extended Data Fig. 2d–g). Western blots demonstrate expression. −ve, untransfected cells.

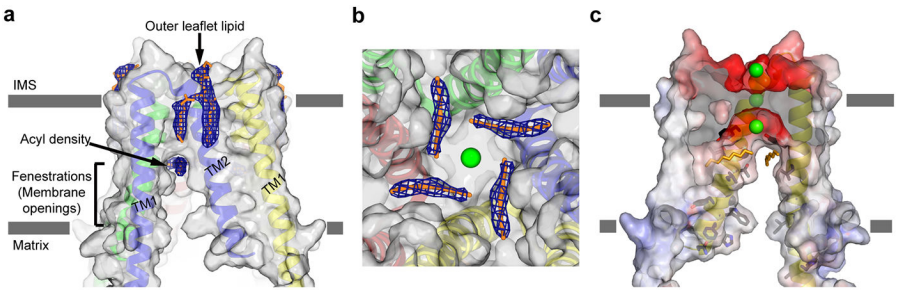

Fig. 5 |. Membrane interactions.

a, Ordered lipids within the transmembrane region. Density (blue mesh, 8σ contour) is ascribed to a lipid of the outer leaflet and an acyl chain within the lateral membrane openings (fenestrations). The partially transparent molecular surface (grey) reveals a ribbon representation of the channel, in which each subunit is coloured uniquely. **b**, Close-up view, orthogonal to **a**, from within the matrix, showing the acyl chain density (site 3 is a green sphere). **c**, The vestibule is hydrophobic. A slice of the molecular surface shown from **a** (the portion facing the viewer is removed) is coloured according to electrostatic potential: light grey regions are neutral; red, −8 kT e^{-1}; blue, +8 kT e^{-1}. Green spheres indicate sites 1–3. One subunit is shown as yellow ribbons with amino acids facing the vestibule drawn as sticks.